analytical chemistry

pubs.acs.org/ac Article

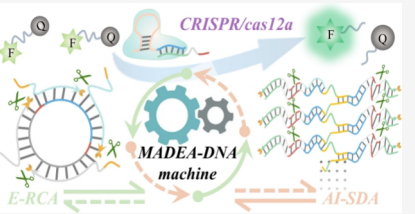
Mutually Activated Dual-Exponential Amplification DNA Machine Enhances Robust CRISPR/Cas12a Feedback Propagation for Ultrasensitive miRNA Detection

Qi Wang, Shuo Yang, Xiumei Chen, Shihui Song, Yan Wu, Yang Li, Xiang Meng, Luyang Dai, Zheng Yang, Hanlin Wu, Juan Xia, and Jianguo Xu*

Cite This: https://doi.org/10.1021/acs.analchem.5c01953 Read Online

ACCESS | Metrics & More | Article Recommendations | Supporting Information

ABSTRACT: Breast cancer (BC) remains a critical global health challenge, necessitating ultrasensitive methods for detecting biomarkers such as miR-155, a key regulator in BC progression. Here, we present a mutually activated dual-exponential amplification DNA machine (MADEA-DNA machine) for ultrasensitive miR-155 detection. This system integrates exponential rolling circle amplification (E-RCA) and autocatalytic incremental strand displacement amplification (AI-SDA), driven by a bidirectional activation mechanism. Target miR-155 initiates E-RCA via a functional primer probe (FPP) or AI-SDA through a functional hairpin probe (FHP), with amplification products cross-activating the counterpart system to establish a self-reinforcing loop. The resultant amplicons further activate CRISPR/Cas12a, enabling the trans-cleavage of fluorescent reporters for signal amplification. The MADEA-DNA machine achieves a detection limit of 1.26 fM, with a dynamic range spanning 5 fM−10 nM, and demonstrates exceptional specificity against mismatched and nontarget miRNAs. Validation in human serum revealed significantly elevated miR-155 levels in BC patients versus healthy donors, corroborated by qRT-PCR. This system combines machine-like operational efficiency, dual-amplification synergy, and CRISPR-enhanced sensitivity, offering a robust platform for liquid biopsy applications in early BC diagnostics.



INTRODUCTION

Breast cancer (BC) remains one of the most prevalent malignancies affecting women globally, with its mortality rate steadily increasing year after year and posing enormous health hazards to women.[1,2] MicroRNAs (miRNAs), short noncoding RNAs regulating post-transcriptional gene expression,[3] have emerged as promising candidates due to their dysregulation in malignancies.[4,5] Among these, miR-155 strongly correlates with BC progression and treatment response.[6] Therefore, the accurate detection of miR-155 is crucial for early diagnosis and subsequent prognostic strategies in BC.[7−9] Nowadays, traditional strategies for quantifying miRNA levels still rely on real-time polymerase chain reaction, Northern blotting, fluorescence in situ hybridization, and microarray methods.[10,11] However, they frequently encounter challenges such as complex operations, high costs, and the need for specialized instruments.[12−15] Given the limitations of the current methods, there is an urgent need to develop innovative techniques for miRNA detection.

The inherent structural and functional properties of nucleic acids enable the creation of advanced DNA-based devices.[16,17] Among these, DNA machines have emerged as particularly prominent, constructed from DNA strands and designed to execute mechanical operations in response to external stimuli.[18−20] This capability renders them exceptionally suitable for developing various biosensing platforms, especially in light of the rapid progress in isothermal nucleic acid amplification techniques.[21−23] Techniques such as rolling circle amplification (RCA), strand-displacement amplification (SDA), and their variants have been extensively developed into versatile DNA machines.[23−25] This development is facilitated by their precise molecular recognition capabilities, the programmable nature of oligonucleotide sequences, and the compatibility with enzymes such as polymerase and endonuclease. Target substances, such as miRNAs, can precisely induce these DNA machines to perform specific programmed actions and amplify target responses through effective signal transduction pathways. Nonetheless, using a single mode of isothermal nucleic acid amplification in constructing DNA machines often does not meet the rigorous demands of clinical diagnostics, such as the need for ultrasensitivity in analyzing human fluid samples. To address this limitation, some researchers have attempted to build DNA machines by combining two or more different isothermal nucleic acid amplification methods to improve target detection sensitivity.[26,27]

Received: April 1, 2025
Revised: June 5, 2025
Accepted: June 6, 2025

Downloaded via SHANGHAI NORMAL UNIV on June 17, 2025 at 00:17:22 (UTC).
See https://pubs.acs.org/sharingguidelines for options on how to legitimately share published articles.

ACS Publications © XXXX American Chemical Society

Despite significant progress in enhancing assay performance by developing advanced DNA machines, their operational efficiency remains suboptimal due to the involvement of multiple oligonucleotide probes. For example, specific DNA machines require more than three oligonucleotides to execute signal amplification pathways. Moreover, while external stimuli, such as target nucleic acids, are often employed to initiate the isothermal amplification process resembling machine-like movement, these target nucleic acids are not recyclable. Additionally, the isothermal amplification products merely act as inducers for signal output and cannot be repurposed to further enhance the isothermal machine-like movement process. Therefore, enhancing the efficiency of the machine-like movement under target stimulation is crucial for improving the assay performance of the DNA machine in miRNA biosensing applications.

Building upon these considerations, we present a mutually activated dual-exponential amplification DNA machine (MADEA-DNA machine) for the ultrasensitive detection of BC-associated biomarkers of miR-155. This innovative system synergistically integrates exponential rolling circle amplification (E-RCA) with autocatalytic incremental strand displacement amplification (AI-SDA). The paradigm-shifting feature of this molecular circuitry lies in its bidirectional activation mechanism: target miR-155 serves as a universal trigger that initiates either (1) the E-RCA module through a single padlock probe recognition or (2) the AI-SDA module via interaction with the functional hairpin probe. Crucially, amplification products from each module cross-activate the counterpart system. Namely, the E-RCA-generated sequences induce AI-SDA cascades, while AI-SDA outputs reciprocally fuel subsequent E-RCA cycles. This intelligent cross-activation architecture establishes a self-reinforcing amplification loop, enabling exponential product accumulation through machine-like operational cycling. The resultant amplicons subsequently serve as programmable activators for the CRISPR/Cas system, enabling sequence-specific recognition by the Cas12a-crRNA complex. Cas12a, a type V-A CRISPR-associated nuclease, specifically cleaves target double-stranded DNA (dsDNA) or single-stranded DNA (ssDNA) when paired with a crRNA.[28−30] Upon activation, the trans-cleavage ability of the CRISPR/Cas12a system degrades ssDNA fluorescent reporters (ssDNA-FR), enabling rapid fluorescence signal transduction. By integrating CRISPR/Cas12a's precise targeting with DNA machines' programmable signal amplification, this system enables ultrasensitive and specific detection. With these features, the MADEA-DNA machine demonstrates enhanced analytical performance, operational efficiency, and clinical utility for precise miRNA quantification in human serum, establishing a new paradigm for nucleic acid detection that is particularly advantageous for liquid biopsy applications.

EXPERIMENTAL SECTION

Materials and Reagents. T4 DNA ligase (5 U/μL; 10× buffer: 400 mM Tris pH 7.8, 100 mM $MgCl_2$, 100 mM DTT, 10 mM ATP) and RNase Inhibitor (40 U/μL) were procured from Beyotime Biotechnology (Shanghai, China). EnGen Lba Cas12a (1 μM; 10× NEBuffer r2.1:500 mM NaCl, 100 mM Tris−HCl, 100 mM $MgCl_2$, 1 mg/mL recombinant albumin, pH 7.9), Klenow fragment (3′-5′ exo-, 5 U/μL; 10× NEBuffer 2:500 mM NaCl, 100 mM $MgCl_2$, 100 mM Tris−HCl, 10 mM DTT, pH 7.9), and Nt.BbvCI (10 U/μL; 10× CutSmart: 200 mM Tris-acetate, 100 mM magnesium acetate, 500 mM potassium acetate, 1 mg/mL BSA, pH 7.9) were obtained from New England Biolabs (Beijing, China). Sangon Biotech (Shanghai, China) supplied dNTPs (25 mM), 10,000× 4S Red Plus, and 10× DNA loading buffer. Additional reagents included a SweScript RT II cDNA Synthesis Kit (Servicebio, Wuhan, China), Servicebio 2× SYBR Green qPCR Master Mix, and HaiGene Biotechnology serum miRNA extraction kit (Harbin, China). High-performance liquid chromatography-purified oligonucleotides (Table S1) were dissolved in 1× TE buffer (Sangon Biotech). All solutions were prepared with nuclease-free water.

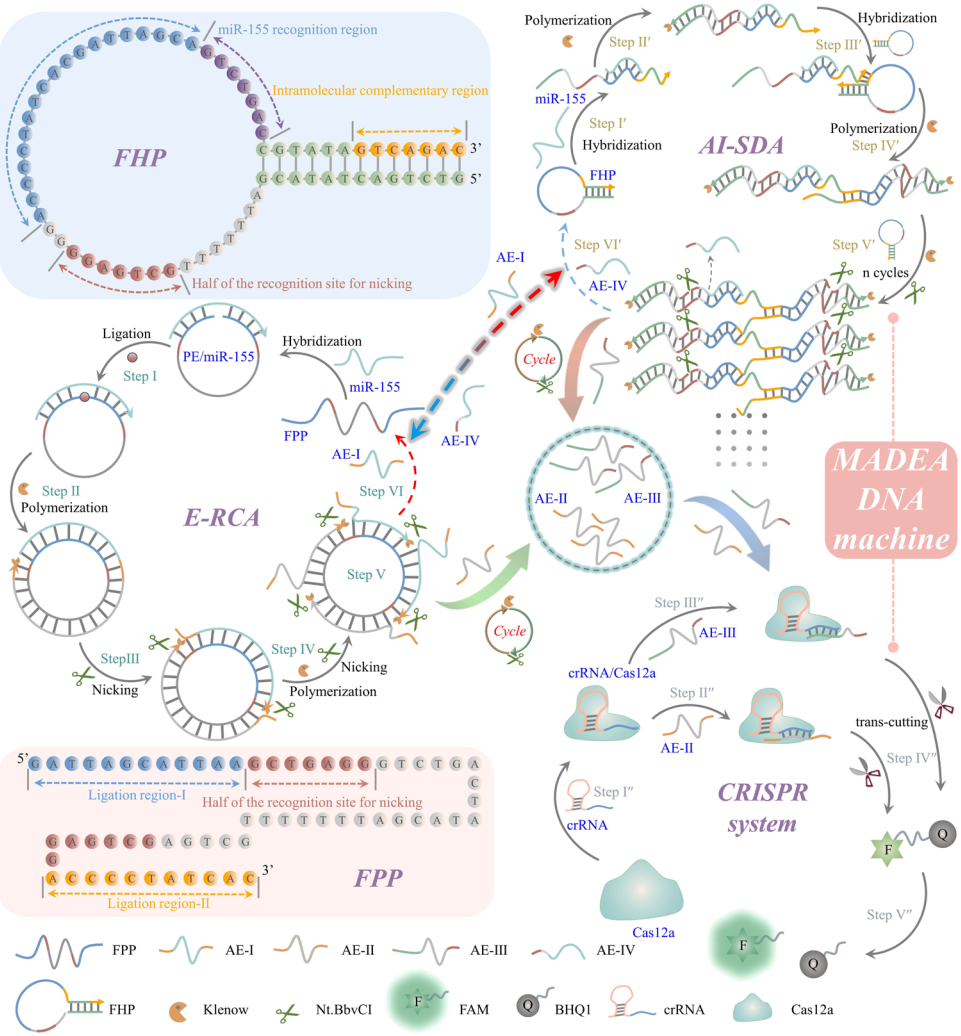
DADM-Based Target MiR-155 Detection. To ensure the stability of its hairpin structure, the functional hairpin probe (FHP) was initially maintained at 95 °C for 5 min. The enzymatic reactions were conducted in a total system volume of 20 μL. To begin with, 2 μL of 2 μM functional primer probe (FPP), 2 μL of miR-155 at a specific concentration, 1 μL of 5 U/μL T4 DNA ligase, 2 μL of 10× T4 ligation buffer, 2 μL of 2 μM FHP, 1 μL of 5 U/μL Klenow fragment polymerase, 2 μL of 10× NEBuffer 2, 1 μL of 10 U/μL Nt.BbvCI, 2 μL of 10× CutSmart, 2 μL of 25 mM dNTPs, and 3 μL of dd-H_2O were incubated at 37 °C for 1 h. Subsequently, the enzyme activity was completely deactivated by subjecting it to a temperature of 65 °C for 10 min. The CRISPR/Cas12a reaction solution was prepared by adding 4 μL of 1 μM Cas12a, 4 μL of 500 nM crRNA, 4 μL of 10× reaction buffer, and 1 μL of 40 U/μL RNase Inhibitor to the above mixture at a temperature of 25 °C for 10 min. Next, 4 μL of a 10 μM solution of FAM- and BHQ1-modified ssDNA-FR was added to the above solution, followed by 3 μL of dd-H_2O. The resulting mixture (40 μL) was then incubated at 37 °C for 30 min. Finally, we added 160 μL of dd-H_2O to the samples and carefully transferred them to a 96-well plate for precise fluorescence recording. It is worth noting that the final concentrations of all oligonucleotide species were determined based on the resulting total volume of the 200 μL solution. Fluorescence measurements were performed utilizing a TECAN Spark multifunctional microplate reading instrument (Zurich, Switzerland). The specific parameters were set as follows: the scan selection was an emission scan with an excitation wavelength of 450 nm and an excitation bandwidth of 20 nm. The emission bandwidth was also set at 20 nm, and the recording range spanned from 500 to 600 nm. The emission wavelength step size was adjusted to 1 nm, with 101 emission scans performed. Finally, the gain was set to 80. The assay performance was assessed by measuring the fluorescence intensity at 520 nm in both the absence and presence of miR-155.

Polyacrylamide Gel Electrophoresis (PAGE) Analysis. To prepare the 12% native-PAGE gel, 5.9 mL of dd-H_2O, 6 mL of 30% acrylamide: bis-acrylamide, 3 mL of 10× TBE buffer, 110 μL of 10% ammonium persulfate, and 10 μL of TEMED were combined at room temperature for approximately 30 min. Each sample well was loaded with a mixture of 20 μL, consisting of a specific volume of the sample, 2 μL of 10× DNA loading buffer, and 3 μL of 100× 4S Red Plus. Subsequently, electrophoresis analysis was conducted employing a Servicebio PW-600 electrophoresis analyzer (Wuhan, China) in a 1× TBE buffer solution at a voltage setting of 80 V for 90 min. Finally, the gel image was captured by using a ChampGel 7000 gel imaging system (Beijing, China).

Extraction of Total RNA from Human Blood. The human blood samples from healthy donors and BC patients

https://doi.org/10.1021/acs.analchem.5c01953
Anal. Chem. XXXX, XXX, XXX−XXX

Scheme 1. Schematic Illustration of the Target-Induced MADEA-DNA Machine Consisting of E-RCA and AI-SDA for miR-155 Signaling



were kindly provided by the Fuyang People's Hospital and approved by the ethics committee of clinical trials of Fuyang People's Hospital (2023byzd219). The human serum was obtained by centrifuging blood samples at 4000 rpm for 15 min. Total RNAs were extracted from the human serum using a serum miRNA extraction kit according to the manufacturer's guidelines. The experiment follows the general procedure outlined below. Initially, 300 μL of human serum was thoroughly mixed with 800 μL of miRNA reagent and incubated at room temperature for 5 min. The above mixture was centrifuged at 13,000 rpm for 5 min, and the resulting supernatant was then combined with 1 mL of isopropanol. The mixed solution was added to the miRNA adsorption column in three separate additions and then centrifuged at 13,000 rpm for 15 s. Next, the miRNA adsorption column was washed successively with 700 μL of 75% isopropanol and 500 μL of anhydrous ethanol by centrifuging at 13,000 rpm for 15 s. The miRNA adsorption column was centrifuged at 13,000 rpm for 2 min. After that, it was incubated at room temperature for another 2 min to ensure the complete removal of ethanol. Finally, the miRNA adsorbed on the column was eluted using RNase-free H_2O. The extracted total miRNAs were quantified using a Thermo Fisher Scientific NanoDrop Spectrophotometer (Vantaa, Finland) at a wavelength of 260 nm. The quantified miRNAs were immediately utilized for cDNA synthesis in reverse transcription reactions.

Reverse Transcription (RT) and Quantitative Reverse Transcription-Polymerase Chain Reaction (qRT-PCR). The reverse transcription reaction was conducted according to the instructions provided in the RT kit manual. To initiate the experiment, 1 μL of 10× gDNA Remover Buffer was added, followed by 1 μL of gDNA Remover, then 2 μL of 250 ng/μL RNA, and finally 6 μL of Nuclease-Free Water. After thorough mixing, the above mixture was incubated at 37 °C for 2 min and then placed on ice for further use. The RT reaction was performed in a 20 μL reaction system, which included 10 μL of the RNA mentioned above, 4 μL of 5× Reaction Buffer, 1 μL of SweScript RT II Enzyme Mix, 1 μL of 100 μM stem-loop reverse transcription primer, and 4 μL of Nuclease-Free Water. The RT protocol involves incubation at 25 °C for 5 min, then at 55 °C for 15 min, and finally at 85 °C for a brief duration of 5 s. The produced cDNA was stored at−80 °C for future experiments. The qRT-PCR reaction system was composed of a 20 μL mixture, which included 10 μL of 2× SYBR Green qPCR Master Mix (None ROX), 1 μL each of 10 μM forward and reverse primers, 2 μL of cDNA solution, and 6 μL of RNase-free H_2O. The amplification process began with an initial denaturation step at 95 °C for 30 s, followed by 40

https://doi.org/10.1021/acs.analchem.5c01953
Anal. Chem. XXXX, XXX, XXX−XXX

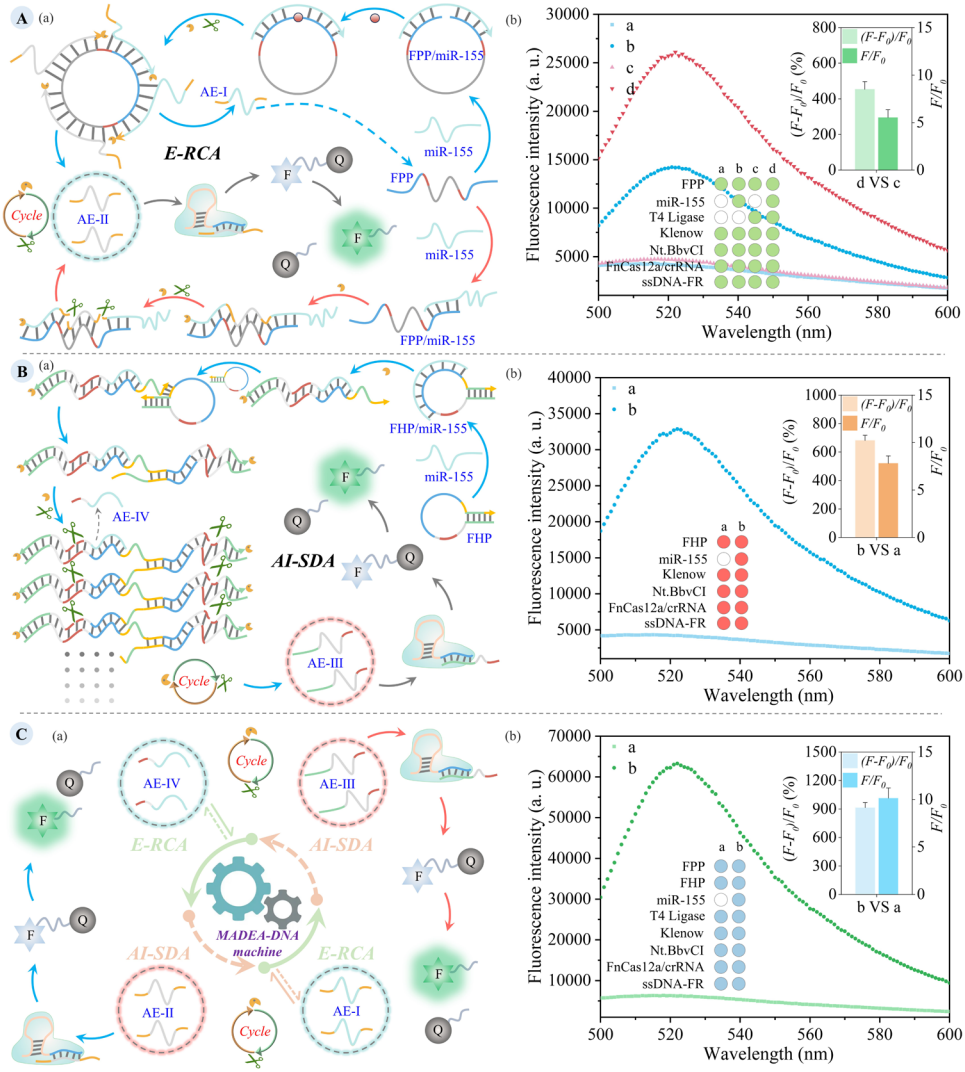


Figure 1. Elucidation of the MADEA-DNA machine approach activation mechanism by miR-155 for CRISPR/Cas12a-mediated trans-cleavage of ssDNA-FR. (A) Operational schematic illustrating the miR-155-activated E-RCA process (panel a) and corresponding fluorescence profiles (panel b). Typical fluorescence was recorded from the unligated FPP before (line a) and after (line b) treatment with miR-155 without T4 ligase. Lines c and d show the results in the presence of T4 ligase, corresponding to the absence and presence of miR-155, respectively. (B) Procedural diagram of miR-155-triggered AI-SDA (panel a) with associated fluorescence progression curves (panel b). System responses include baseline fluorescence from nonactivated AI-SDA (line a) and amplified fluorescence from miR-155-activated AI-SDA (line b). (C) Integrated MADEA-DNA machine operational workflow combining E-RCA and AI-SDA modules under miR-155 activation (panel a) with corresponding multiplexed fluorescence readouts (panel b). Signal amplification metrics were quantified through background fluorescence (line a) versus that of the target-activated MADEA-DNA machine (line b). The signal enhancement percentage was calculated as $[(F - F_0/F_0) \times 100\%]$, while (F/F_0) represents the signal-to-noise ratio (S/N). F and F_0 represent the peak fluorescent signals in the presence and absence of target miR-155, respectively. The data represent the average values obtained from three repeated experiments, with error bars indicating the standard deviations. Detailed experimental parameters: FPP = FHP = miR-155 = 20 nM, T4 Ligase = Klenow = 25 U/mL, Nt.BbvCI = 50 U/mL, RNase Inhibitor = 200 U/mL, Cas12a = 20 nM, crRNA = 10 nM, dNTPs = 250 μM, ssDNA-FR = 200 nM, enzymatic reaction time = 60 min, and trans-cleave time = 30 min.

cycles of denaturation at 95 °C for 15 s and annealing/extension at 55 °C for 30 s. The expression of miR-155 was quantified by calculating the ΔCq values ($\Delta Cq = Cq_{\text{miR-155}} - Cq_{\text{U6}}$). qRT-PCR analysis was performed in triplicate for each sample, and the primer sequences utilized are documented in Table S1. qRT-PCR reactions were performed in triplicate using a Bio-Rad CFX Connect Real-Time PCR System (California, USA). The reaction temperature was consistently regulated via a Bio-Rad T100 thermal cycler system (Hercules, USA).

RESULTS AND DISCUSSION

Working Principle of the Target-Induced MADEA-DNA Machine. The rational design of FPP and FHP is a prerequisite to constructing the target-induced MADEA-DNA machine. In our study, the FPP is designed with two target recognition regions at its termini and two Nt.BbvCI endonuclease recognition sites in its central region. The FHP comprises a target recognition fragment, an Nt.BbvCI recognition sequence, and two identical "GTCAGAC" sequences. These two components are employed to initiate E-RCA and AI-SDA, respectively. As illustrated in Scheme 1, the operation begins when the target miRNA (miR-155) acts

https://doi.org/10.1021/acs.analchem.5c01953
Anal. Chem. XXXX, XXX, XXX−XXX

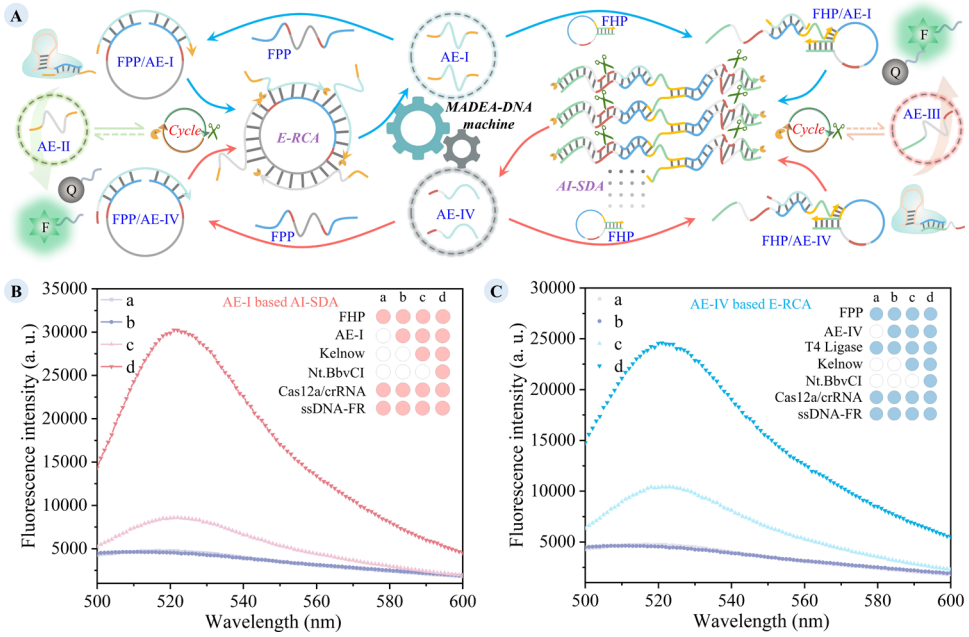


Figure 2. Schematic representation and experimental validation of the interactive operation between E-RCA and AI-SDA components in the MADEA-DNA machine. (A) Illustration depicting the mutual induction of the amplification processes E-RCA and AI-SDA. (B) Fluorescent measurement results of (a) FHP, (b) FHP and AE-I, (c) FHP, AE-I, and Klenow, and (d) FHP, AE-I, Klenow, and Nt.BbvCI to activate CRISPR/Cas12a for trans-cleavage of ssDNA-FR. (C) Fluorescent measurement results of (a) FPP and T4 ligase, (b) FPP, T4 ligase, and AE-IV, (c) FPP, T4 ligase, AE-IV, and Klenow, (d) FPP, T4 ligase, AE-IV, Klenow, and Nt.BbvCI will activate CRISPR/Cas12a for trans-cleavage of ssDNA-FR. Detailed experimental parameters: FPP = FHP = AE-I = AE-IV = 20 nM, T4 Ligase = Klenow = 25 U/mL, Nt.BbvCI = 50 U/mL, RNase Inhibitor = 200 U/mL, Cas12a = 20 nM, crRNA = 10 nM, dNTPs = 250 μM, ssDNA-FR = 200 nM, enzymatic reaction time = 60 min, and trans-cleave time = 30 min.

as a trigger, binding to either the FPP or FHP to form FPP/miR-155 or FHP/miR-155 duplex complexes. For the FPP/miRNA complex, T4 DNA ligase facilitates the ligation of the FPP's 5′ and 3′ termini, resulting in a closed circular template. This circular FPP then undergoes strand replication, initiated by extending the miRNA's 3′ end, generating two complete Nt.BbvCI recognition sites. Upon encountering Nt.BbvCI, the replicated circular dsDNA is cleaved at these sites, producing the corresponding nick sites that serve as binding points for the Klenow fragment polymerase. The polymerase extends from the nick, working in tandem with Nt.BbvCI to drive a machine-like cycle of strand polymerization, cleavage, and displacement. This process continuously generates two ssDNA products: activation element-I (AE-I), which contains the miR-155 recognition sequence, and activation element-II (AE-II), which is complementary to the crRNA. Notably, both AE-I and AE-II are recycled in subsequent rounds of pairing, ligation, polymerization, cleavage, and displacement, thereby sustaining the machine-like operation. Furthermore, AE-I can trigger AI-SDA by interacting with the FPP (described below). At the same time, AE-II hybridizes with crRNA/Cas12, activating the CRISPR system to cleave ssDNA-FR and release a fluorescent signal nonspecifically.

In parallel, when the FHP/miR-155 complex is formed, the extension of the miRNA's 5′ end using FHP as a template generates a complete Nt.BbvCI recognition site. Consequently, Nt.BbvCI specifically cleaves the upper strand of the resulting dsDNA at this site, creating a nick that serves as a primer binding site for further extension by the Klenow fragment polymerase. This results in the displacement of the downstream strand, producing many amplicons termed activation element-III (AE-III) and displacing the extended miR-155, which is designated activation element-IV (AE-IV). Simultaneously, the stem region of the FHP is entirely liberated, releasing its 3′ end to hybridize with another FHP molecule. Under the action of the Klenow fragment polymerase, the extension of the liberated 3′ end using the second FHP as a template occurs. This process not only continues to generate additional Nt.BbvCI recognition sites that are used for further nicking and accumulation of AE-III, and they also facilitate repeated intramolecular hybridizations, promoting robust DNA replication. As a result, AI-SDA is autonomously driven by multiple concurrent machine-like movements at numerous nick sites to maximize AE-III production. Similar to AE-I and AE-II, AE-III not only acts as a stimulus to further enhance the isothermal machine-like motion but also binds with crRNA to activate the CRISPR/Cas12a system, leading to the non-specific cleavage of ssDNA-FR. Meanwhile, AE-IV serves a dual role by rehybridizing with FHP to promote AI-SDA further and by being recycled to activate E-RCA. The target-induced MADEA-DNA machine is successfully constructed by integrating the mechanical operations of E-RCA and AI-SDA, providing a powerful fluorescent signal feedback mechanism to indicate both the presence and concentration of target miRNAs. Theoretically, this DNA machine continues to operate until all FPP and FHP components are exhausted. In contrast, in the absence of miR-155, the FPP cannot be ligated. The 3′ terminus of the FHP remains sequestered within its stem structure, thereby preventing the initiation of E-RCA and AI-SDA and ensuring a low background signal. Moreover, to prevent off-target interactions, FPP and FHP are designed with noncomplementary sequences and enhanced structural stability. Without targets, they remain locked in inactive

https://doi.org/10.1021/acs.analchem.5c01953
Anal. Chem. XXXX, XXX, XXX−XXX

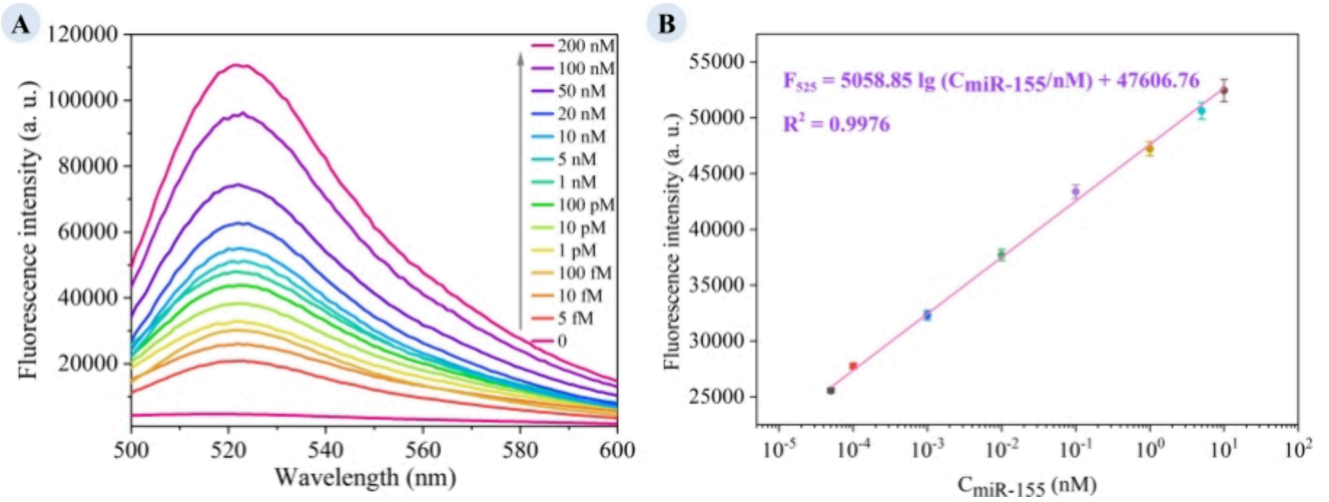


Figure 3. (A) Fluorescent responses of the MADEA-DNA machine to different concentrations of target miR-155, ranging from 0 to 200 nM. (B) Regression analysis plot shows the relationship between the miR-155 concentration and peak fluorescence intensity. Error bars are obtained from three repetitive tests. Detailed experimental parameters: FPP = FHP = 20 nM, T4 Ligase = Klenow = 25 U/mL, Nt.BbvCI = 50 U/mL, RNase Inhibitor = 200 U/mL, Cas12a = 20 nM, crRNA = 10 nM, dNTPs = 250 μM, ssDNA-FR = 200 nM, enzymatic reaction time = 60 min, and trans-cleave time = 30 min.

conformations, thereby blocking enzymatic recognition and initiation of amplification.

Feasibility Demonstration of MADEA-DNA Machine in Detecting miR-155. In this study, we demonstrated the feasibility of the MADEA-DNA machine for detecting miR-155 using two key components: E-RCA and AI-SDA. Initially, we evaluated the performance of E-RCA in detecting miR-155 independently. The evaluation involved hybridizing FPP with miR-155 and connecting FPP with the T4 DNA ligase. As shown in panel a of Figure 1A, the CRISPR/Cas12 system was activated through E-RCA in the presence of Klenow fragment polymerase and Nt.BbvCI endonuclease. Without T4 DNA ligase, miR-155 can still interact with unblocked FPP through the combined action of Klenow fragment polymerase and Nt.BbvCI endonuclease (lane b). However, in this process, only AE-II can undergo amplification, while the production of AE-I is hindered, leading to compromised signal enhancement. Panel b of Figure 1A shows a significant enhancement in the fluorescence signal (lane d) due to the presence of miR-155, resulting in a 453.47% increase in signal intensity $[(F - F_0/F_0) \times 100\%]$ compared to its absence (lane c), leading to a signal-to-noise ratio (S/N, F/F_0) of 5.53. Here, F and F_0 represent the peak fluorescence signals recorded in the presence and absence of the target miR-155, respectively. Additionally, E-RCA characteristics were examined via gel electrophoresis (Figure S1A).

To assess the independent performance of AI-SDA in detecting miR-155, we initiated AI-SDA by incubating FHP with the target miR-155. Panel a of Figure 1B illustrates this process. Panel b of Figure 1B shows that the absence of miR-155 results in a relatively low fluorescence intensity (lane a). At the same time, its addition significantly increases the signal (lane b) by approximately 680.93%, improving the S/N ratio to 7.81. Detailed characterization of AI-SDA through gel electrophoresis is provided in Figure S1B. To evaluate the overall efficacy of the MADEA-DNA machine, we used both FPP and FHP to detect the target miR-155 (panel a of Figure 1C). As shown in panel b of Figure 1C, the presence of miR-155 leads to a significantly higher signal intensity. The above results demonstrated the feasibility of the MADEA-DNA machine in detecting miR-155 and indirectly suggested a close interaction between E-RCA and AI-SDA. Furthermore, we synthesized AE-II and AE-III to demonstrate the activation of the CRISPR/Cas12a system by both E-RCA and AI-SDA products (Figure S2).

Mechanistic Validation of Mutually Activated Dual-Exponential Amplification. As previously described, the MADEA-DNA machine employs a distinctive mutually activated interplay between its core components, E-RCA and AI-SDA, enabling mutual activation to drive exponential amplification. This reciprocal activation mechanism operates through a feed-forward loop where E-RCA amplification products initiate AI-SDA processes, while AI-SDA products conversely stimulate nicked E-RCA amplification (Figure 2A). We conducted sequential verification experiments focusing on both interaction pathways to validate this operational principle systematically. To confirm the capacity of E-RCA products to trigger AI-SDA, a synthetic AE-I (an E-RCA-derived amplicon) was introduced to interact with FHPs. As depicted in Figure 2B, fluorescence monitoring revealed no signal elevation when FHP was tested alone (line a) or in the presence of AE-I without enzymatic treatment (line b). Notably, incubation of the FHP/AE-I duplex with Klenow (line c) induced modest fluorescence enhancement, which was attributed to the partial formation of elongated dsDNA through dimer-directed replication. This dsDNA product facilitated crRNA-guided CRISPR/Cas12a activation, causing limited nonspecific cleavage of ssDNA-FR. Subsequently, combinatorial treatment with Klenow and Nt.BbvCI (line d) generated a dramatic fluorescence surge, demonstrating efficient CRISPR/Cas12a activation through amplified cleavage activity. These results demonstrate that AE-I effectively functions as an exchange primer to activate the AI-SDA cascade.

To establish the reciprocal activation mechanism, synthetic AE-IV (an AI-SDA-derived product) was evaluated for its ability to initiate E-RCA processes. Initial testing showed no detectable fluorescence when FPP was assayed alone (Figure

https://doi.org/10.1021/acs.analchem.5c01953
Anal. Chem. XXXX, XXX, XXX−XXX

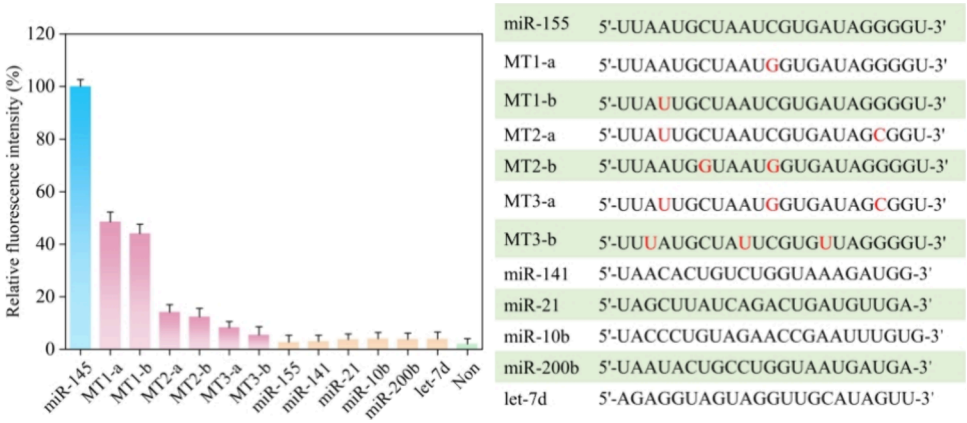


Figure 4. Different target analytes cause peak fluorescent intensities of the MADEA-DNA machine. The data were presented as mean ± standard error of the mean, and error bars were obtained from three repetitive tests. Detailed experimental parameters: FPP = FHP= miR-155 = MT1-a = MT1-b = MT2-a = MT2-b = MT3-a = MT3-b = miR-141 = miR-21 = miR-10b = miR-200b = let-7d = 20 nM, T4 Ligase = Klenow = 25 U/mL, Nt.BbvCI = 50 U/mL, RNase Inhibitor = 200 U/mL, Cas12a = 20 nM, crRNA = 10 nM, dNTPs = 250 μM, ssDNA-FR = 200 nM, enzymatic reaction time = 60 min, and trans-cleave time = 30 min.

2C, line a) or after AE-IV hybridization without enzymatic processing (line b). Following ligation treatment, FPP/AE-IV complexes incubated with Klenow alone (line c) exhibited measurable signal amplification through partial dsDNA synthesis. Remarkably, the concurrent application of Klenow and Nt.BbvCI (line d) produced substantially intensified fluorescence, confirming efficient nicking-enzyme-assisted RCA initiation. This progressive signal amplification pattern conclusively verifies that AE-IV is a competent primer for E-RCA initiation, completing the bidirectional activation circuit. The collective experimental evidence from both activation pathways supports the core design principle of the MADEA-DNA machine, which is to establish a self-sustaining amplification loop through a reciprocal product exchange between E-RCA and AI-SDA components. This mutually reinforcing interaction provides the foundation for achieving exponential amplification kinetics in the system.

Stimulus−Response Evaluation of the DNA Machine for Detecting Various Concentrations of Target miRNA-155. DNA machines with superior signal amplification capacity demonstrate significant potential for early disease diagnostics and therapeutic monitoring. A stimulus-response evaluation of the MADEA-DNA machine system was performed through quantitative analysis of miR-155 across concentrations spanning 0 to 200 nM under optimized conditions (Figure S3). Fluorescence kinetic analysis revealed a concentration-dependent enhancement of peak fluorescence intensities (Figure 3A). Log−linear regression analysis established the quantitative relationship: F_{525} = 5058.85 lg($C_{miR\text{-}155}$/nM) + 47606.76 (R^2 = 0.9976) over the dynamic range of 5 fM to 10 nM (Figure 3B). The limit of detection (LOD) calculated via 3σ methodology (n = 10 blank replicates) reached 1.26 fM. Compared with most of the isothermal amplification techniques reported in the past (Table S2), such as exponential amplification-triggered DNA walkers (LOD: 5.2 fM) and duplex-specific nuclease-assisted CRISPR/Cas12a strategy (2.4 pM), the MADEA-DNA machine achieves a comparable LOD of 1.26 fM without relying on nanomaterials or multistep target enrichment. By integrating dual-exponential amplification (8 orders of magnitude) and CRISPR-Cas12a feedback, this system simplifies workflows while maintaining ultrasensitivity, outperforming single-amplification strategies like dual-DNA machine based on RCA (10 fM) or palindrome-mediated SDA (50 pM). This enhanced sensitivity originates from the programmed cross-priming amplification mechanism that progressively activates CRISPR/Cas12a trans-cleavage activity in miRNA signal transduction.

External Stimulus Specificity Study. External stimulus specificity is vital to verify whether the DNA machine's activation is exclusively triggered by its intended stimulus. This specificity helps minimize false positives and enhances the detection accuracy for biomedical applications. Given the documented sequence homology among miRNA family members, stringent specificity is essential for accurate molecular diagnostics. An analysis was conducted using the MADEA-DNA machine approach to compare synthetic mismatched miRNA targets, including MT1 (single-base mismatch), MT2 (two-base mismatch), and MT3 (three-base mismatch), as well as synthetic nontarget miRNAs such as miR-141, miR-21, miR-10b, miR-200b, and let-7d, against miR-155. In our design, MT1, MT2, MT3, and MT4 were randomly designed with varying numbers of mutated bases. Subgroups such as MT1-a and MT1-b share the same mutation count but differ in mutation positions. Nontarget miRNAs were also deliberately selected to comprehensively evaluate specificity. As shown in Figure 4, the normalized fluorescence intensities at 525 nm showed significant differences. Compared with miR-155, the MT1 (MT1-a and MT1-b) displayed 44.05−48.52% relative fluorescence intensity. The MT2 (MT2-a and MT2-b) exhibited 12.37−14.16% residual signal, whereas the MT3 (MT3-a and MT3-b) retained only 5.51−8.31%. Nontarget species maintained <3% signal intensity equivalent to background levels. The significant difference in signal between target miRNA and nontargets confirms the high specificity of our proposed DNA machine.

Capability of DNA Machine To Sense Target Stimulus in Human Serum. The collection of human serum is straightforward and minimally invasive, allowing for repeated sampling and routine clinical testing. Circulating miRNAs in human serum hold substantial diagnostic potential. MiR-155 is typically up-regulated in the blood of BC patients compared to healthy individuals, making its monitoring crucial for diagnosis, prognosis, and pathology.[31,32] To evaluate the potential of the

https://doi.org/10.1021/acs.analchem.5c01953
Anal. Chem. XXXX, XXX, XXX−XXX

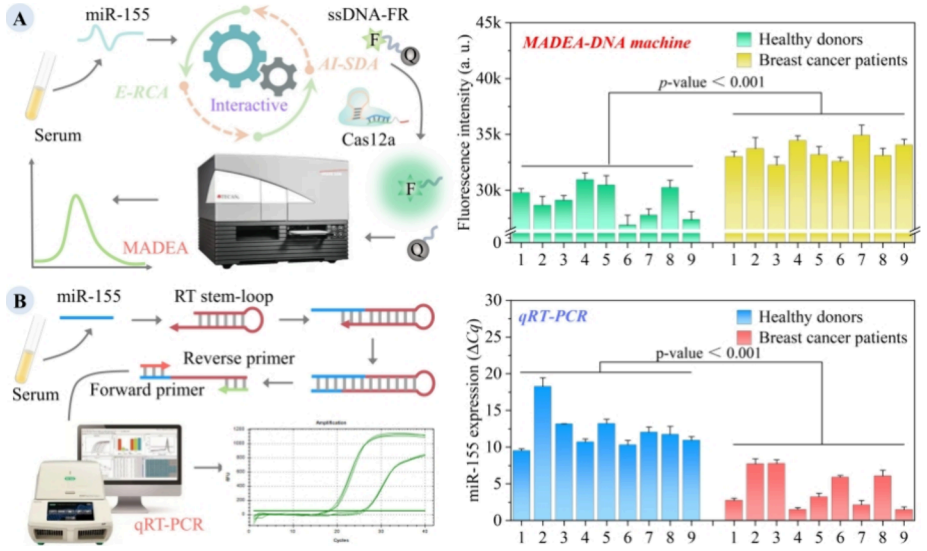


Figure 5. Diagnostic significance of miR-155 upregulation in sera from breast cancer patients. (A) MADEA-DNA machine-based fluorescence quantification of miR-155 levels in BC patients versus healthy donors. (B) qRT-PCR confirmation showing significant ΔCq differences between healthy individuals and BC patients. The data represent the average values obtained from three repeated experiments, with error bars indicating the standard deviations. Detailed experimental parameters: FPP = FHP = 20 nM, T4 Ligase = Klenow = 25 U/mL, Nt.BbvCI = 50 U/mL, RNase Inhibitor = 200 U/mL, Cas12a = 20 nM, crRNA = 10 nM, dNTPs = 250 μM, ssDNA-FR = 200 nM, enzymatic reaction time = 60 min, and trans-cleave time = 30 min.

MADEA-DNA machine strategy for detecting miR-155 in actual samples, we tested serum samples from both healthy donors and BC patients. Before using the MADEA-DNA machine for human serum analysis, pretreatment procedures, such as annealing and dilution, were conducted to minimize protein interference with detection efficiency. As shown in Figure 5A, the MADEA-DNA machine was used to measure miR-155 levels in human serum, revealing significantly higher fluorescence intensity in the BC patient group compared to the healthy donor group. To validate the reliability of the MADEA-DNA machine, we employed qRT-PCR to analyze miR-155 expression in human serum. Figure 5B shows that ΔCq values were consistently lower in the patient group than in the healthy group, indicating a higher miR-155 expression in BC patients. These results suggest that the MADEA-DNA machine is robust and reliable, offering a promising platform for monitoring clinical miRNA markers. Moreover, these findings align with the existing literature on the upregulation of miR-155 in cancer patients' body fluids, particularly blood, confirming its practical value.[32]

CONCLUSIONS

In summary, we have developed a MADEA-DNA machine for a robust and ultrasensitive platform for detecting miR-155. The MADEA-DNA machine represents a paradigm shift in nucleic acid detection, synergizing dual-exponential amplification with CRISPR/Cas12a feedback for ultrasensitive miRNA-155 quantification. The AE-I generated by E-RCA activates AI-SDA, and the AE-IV produced by AI-SDA subsequently provides feedback to the E-RCA, forming a closed-loop amplification circuit. This bidirectional signal transmission not only enhances amplification efficiency but also resolves the issue of signal attenuation caused by single-path dependence in unidirectional systems. The DNA machine achieves exponential signal amplification by utilizing cross-activation between E-RCA and AI-SDA, achieving a detection limit of 1.26 fM and high specificity against closely related miRNA analogs. Its clinical utility was validated through robust discrimination of miR-155 levels in BC patient sera, aligned with qRT-PCR results. Integrating autonomous machine-like operations, recyclable amplification elements, and CRISPR-mediated signal transduction overcomes the limitations of single-amplification methods, ensuring low background and high operational efficiency. Although this strategy involves complex probe design and dual-enzyme optimization, presenting challenges in standardization and cost efficiency, it significantly enhances the sensitivity of miRNA detection and provides a versatile framework for molecular diagnostics in complex biological matrices. This highlights its potential applications in early cancer detection and personalized medicine.

ASSOCIATED CONTENT

Supporting Information

The Supporting Information is available free of charge at https://pubs.acs.org/doi/10.1021/acs.analchem.5c01953.

Gel electrophoresis characterization, optimization of experimental conditions, oligonucleotide sequences, and method comparison (PDF)

AUTHOR INFORMATION

Corresponding Author

Jianguo Xu − *Jiaxing Key Laboratory of Molecular Recognition and Sensing, College of Biological and Chemical Engineering, Jiaxing University, Jiaxing 314001, P. R. China;* orcid.org/0000-0002-0187-2623; Email: jgxu0816@163.com

Authors

Qi Wang − *Key Laboratory of Embryo Development and Reproductive Regulation, Anhui Province Key Laboratory of Pollution Damage and Biological Control for Huaihe River Basin, School of Biological and Food Engineering, Fuyang Normal University, Fuyang, Anhui 236037, P. R. China;* orcid.org/0000-0002-5035-9746

https://doi.org/10.1021/acs.analchem.5c01953
Anal. Chem. XXXX, XXX, XXX−XXX

Shuo Yang − *Key Laboratory of Embryo Development and Reproductive Regulation, Anhui Province Key Laboratory of Pollution Damage and Biological Control for Huaihe River Basin, School of Biological and Food Engineering, Fuyang Normal University, Fuyang, Anhui 236037, P. R. China*
Xiumei Chen − *Key Laboratory of Embryo Development and Reproductive Regulation, Anhui Province Key Laboratory of Pollution Damage and Biological Control for Huaihe River Basin, School of Biological and Food Engineering, Fuyang Normal University, Fuyang, Anhui 236037, P. R. China*
Shihui Song − *Key Laboratory of Embryo Development and Reproductive Regulation, Anhui Province Key Laboratory of Pollution Damage and Biological Control for Huaihe River Basin, School of Biological and Food Engineering, Fuyang Normal University, Fuyang, Anhui 236037, P. R. China*
Yan Wu − *Key Laboratory of Embryo Development and Reproductive Regulation, Anhui Province Key Laboratory of Pollution Damage and Biological Control for Huaihe River Basin, School of Biological and Food Engineering, Fuyang Normal University, Fuyang, Anhui 236037, P. R. China*
Yang Li − *Key Laboratory of Embryo Development and Reproductive Regulation, Anhui Province Key Laboratory of Pollution Damage and Biological Control for Huaihe River Basin, School of Biological and Food Engineering, Fuyang Normal University, Fuyang, Anhui 236037, P. R. China*
Xiang Meng − *Key Laboratory of Embryo Development and Reproductive Regulation, Anhui Province Key Laboratory of Pollution Damage and Biological Control for Huaihe River Basin, School of Biological and Food Engineering, Fuyang Normal University, Fuyang, Anhui 236037, P. R. China*
Luyang Dai − *Key Laboratory of Embryo Development and Reproductive Regulation, Anhui Province Key Laboratory of Pollution Damage and Biological Control for Huaihe River Basin, School of Biological and Food Engineering, Fuyang Normal University, Fuyang, Anhui 236037, P. R. China*
Zheng Yang − *Key Laboratory of Embryo Development and Reproductive Regulation, Anhui Province Key Laboratory of Pollution Damage and Biological Control for Huaihe River Basin, School of Biological and Food Engineering, Fuyang Normal University, Fuyang, Anhui 236037, P. R. China;* orcid.org/0000-0002-7140-2416
Hanlin Wu − *Medical Laboratory Department, Fuyang People's Hospital, Fuyang, Anhui 236037, P. R. China*
Juan Xia − *Key Laboratory of Embryo Development and Reproductive Regulation, Anhui Province Key Laboratory of Pollution Damage and Biological Control for Huaihe River Basin, School of Biological and Food Engineering, Fuyang Normal University, Fuyang, Anhui 236037, P. R. China*

Complete contact information is available at: https://pubs.acs.org/10.1021/acs.analchem.5c01953

Author Contributions

All authors have given approval to the final version of the manuscript.

Notes

The authors declare no competing financial interest.

■ ACKNOWLEDGMENTS

This work was financially supported by the Anhui Provincial Natural Science Foundation (2024AH040206 and 2022AH051335), the Jiaxing Science and Technology Program-Social Development Special Project (2025BS009), the Biological and Medical Sciences of Applied Summit Nurturing Disciplines in Anhui Province (202313), the Fuyang Normal University science research project (2024KYQD0037 and HX2024149000), the National Innovation Training Program for College Students (S202410371095), and the Health Research Project of Anhui Province (AHWJ2022c024).

■ REFERENCES

(1) Fidler, M. M.; Bray, F.; Soerjomataram, I. *Scand. J. Public Health* **2018**, *46* (1), 27−36.
(2) Bray, F.; Ferlay, J.; Soerjomataram, I.; Siegel, R. L.; Torre, L. A.; Jemal, A. *CA. Cancer J. Clin.* **2018**, *68* (6), 394−424.
(3) Gebert, L. F. R.; MacRae, I. J. *Nat. Rev. Mol. Cell Biol.* **2019**, *20* (1), 21−37.
(4) Kim, S.; Kim, S.; Chang, H. R.; Kim, D.; Park, J.; Son, N.; Park, J.; Yoon, M.; Chae, G.; Kim, Y.-K. *Nat. Commun.* **2021**, *12* (1), 5057.
(5) Filipowicz, W.; Bhattacharyya, S. N.; Sonenberg, N. *Nat. Rev. Genet.* **2008**, *9* (2), 102−114.
(6) Grimaldi, A. M.; Incoronato, M. *Cancers* **2019**, *11* (7), 901.
(7) Magen, I.; Yacovzada, N. S.; Yanowski, E.; Coenen-Stass, A.; Grosskreutz, J.; Lu, C.-H.; Greensmith, L.; Malaspina, A.; Fratta, P.; Hornstein, E. *Nat. Neurosci.* **2021**, *24* (11), 1534−1541.
(8) Moon, J.; Liu, C. *Nat. Commun.* **2023**, *14* (1), 7504.
(9) Dong, Y.; Gao, Q.; Chen, Y.; Zhang, Z.; Du, Y.; Liu, Y.; Zhang, G.; Li, S.; Wang, G.; Chen, X. *Nat. Commun.* **2023**, *14* (1), 2540.
(10) Yang, F.; Lu, H.; Meng, X.; Li, L.; Dai, W.; Yang, L.; Zhang, R.; Dong, H.; Zhang, X. *Coord. Chem. Rev.* **2023**, *487*, No. 215157.
(11) Hunt, E. A.; Broyles, D.; Head, T.; Deo, S. K. *Annu. Rev. Anal. Chem.* **2015**, *8* (1), 217−237.
(12) Raymond, C. K.; Roberts, B. S.; Garrett-Engele, P.; Lim, L. P.; Johnson, J. M. *RNA* **2005**, *11* (11), 1737−1744.
(13) Várallyay, E.; Burgyán, J.; Havelda, Z. *Nat. Protoc.* **2008**, *3* (2), 190−196.
(14) Tao, Y.; Zhou, X.; Sun, L.; Lin, D.; Cai, H.; Chen, X.; Zhou, W.; Yang, B.; Hu, Z.; Yu, J. *Nat. Commun.* **2023**, *14* (1), 443.
(15) Martino, S.; Tammaro, C.; Misso, G.; Falco, M.; Scrima, M.; Bocchetti, M.; Rea, I.; De Stefano, L.; Caraglia, M. *Int. J. Mol. Sci.* **2023**, *24* (9), 7762.
(16) Zhang, T.; Tian, T.; Lin, Y. *Adv. Mater.* **2022**, *34* (46), No. 2107820.
(17) Yu, F.; Wang, Y.; Yu, C.; Zhang, W.; Bai, X. *Journal of Analysis and Testing* **2024**, *8* (2), 237−244.
(18) Wang, Q.; Li, W.; Xia, J.; Wu, H.; Wu, L.; Xu, J. *Sensor. Actuat. B-Chem.* **2022**, *363*, No. 131858.
(19) Xia, J.; Liu, Z.; Gao, S.; Wang, Q.; Xu, J.; Wu, H. *Anal. Chem.* **2022**, *94* (46), 16132−16141.
(20) Wang, Q.; Zhou, T.; Xue, D.; Yang, H.; Sui, Z.; Yuan, X.; Xu, J. *Chem. Commun.* **2024**, *60* (21), 2910−2913.
(21) Long, X.; Luo, T.; Yuan, P.; Gan, Y.; Liu, H.; Deng, Z.; Ding, J.; Gong, Z.; Yang, Y.; Zhong, S. *Anal. Chem.* **2023**, *95* (37), 13872−13879.
(22) Yan, H.; Wen, Y.; Tian, Z.; Hart, N.; Han, S.; Hughes, S. J.; Zeng, Y. *Nat. Biomed. Eng.* **2023**, *7* (12), 1583−1601.
(23) Xu, J.; Zhou, T.; Xue, D.; Sui, Z.; Yang, H.; Yuan, X.; Wang, Q. *Chem. Commun.* **2024**, *60* (40), 5314−5317.
(24) Zhang, L.; Zhu, J.; Li, T.; Wang, E. *Anal. Chem.* **2011**, *83* (23), 8871−8876.
(25) Wang, M.-Y.; Jing, W.-J.; Wang, L.-J.; Jia, L.-P.; Ma, R.-N.; Zhang, W.; Shang, L.; Li, X.-J.; Xue, Q.-W.; Wang, H.-S. *Biosens. Bioelectron.* **2023**, *226*, No. 115116.
(26) Wang, Q.; Xia, J.; Yang, C.; Chen, X.; Chen, B.; Li, Y.; Huang, H.; Lin, B.; Guo, L.; Xu, J. *Anal. Chem.* **2024**, *96* (35), 14205−14214.
(27) Qin, P.; Yao, L.; Xu, J.; Liu, G.; Chen, W. *Chem. Commun.* **2019**, *55* (95), 14367−14370.
(28) Xu, L.; Liu, S.; Huang, Z.; Pei, X.; Li, S.; He, Y.; Tong, Y.; Liu, G. *Journal of Analysis and Testing* **2025**, *9* (1), 153−159.
(29) Feng, Z.; Liu, R.; Yang, E.; Lian, R.; Zhang, J. *Journal of Analysis and Testing* **2025**, *9* (1), 1−11.

(30) Sui, Z.; Chen, B.; Zhao, J.; Yang, H.; Guo, L.; Xu, J. *Anal. Chem.* **2025**, *97* (8), 4668−4677.
(31) Jiang, S.; Zhang, H.; Lu, M.; He, X.; Li, Y.; Gu, H.; Liu, M.; Wang, E. *Cancer Res.* **2010**, *70* (8), 3119−3127.
(32) Grimaldi, A. M.; Nuzzo, S.; Condorelli, G.; Salvatore, M.; Incoronato, M. *Int. J. Mol. Sci.* **2020**, *21* (16), 5834.

https://doi.org/10.1021/acs.analchem.5c01953
Anal. Chem. XXXX, XXX, XXX−XXX